

# Is One of the Least Coordinating Anions Suitable to Serve as Electrolyte Salt for Magnesium-Ion Batteries?

Alexei Schmidt,<sup>[a]</sup> Hendrik Koger,<sup>[a]</sup> Antoine Barthélémy,<sup>[a]</sup> Gauthier Studer,<sup>[b]</sup> Birgit Esser,<sup>[b]</sup> and Ingo Krossing<sup>\*[a]</sup>

Weakly coordinating anions (WCAs) are considered promising candidates for application as electrolytes in multivalent post-lithium batteries. One strong candidate as electrolyte salt for Mg battery application is  $[\text{Mg}(\text{L})_x][\text{Al}(\text{OR}^{\text{F}})_4]_2$  ( $\text{L} = \text{MeCN}$  (acetonitrile), DME (1,2-dimethoxyethane);  $x = 3, 6$ ;  $\text{R}^{\text{F}} = \text{C}(\text{CF}_3)_3$ ) that contains  $[\text{Al}(\text{OR}^{\text{F}})_4]^-$  as one of the least coordinating WCAs known. Here we present a novel synthetic route, for which vibrational, NMR and XRD analyses show the formation of a clean, pristine electrolyte salt without the common contaminants found in published synthetic routes. The electrochemistry of this pristine and pure  $[\text{Mg}(\text{DME})_3][\text{Al}(\text{OR}^{\text{F}})_4]_2$  electrolyte (0.2 M in DME) was investigated via cyclic voltammetry (CV). In contrast to previous publications using impure materials, the CV showed no sign for Mg deposition from the pristine

electrolyte for all conditions tested. This also holds when including the additives LiCl, NaCl, MgCl<sub>2</sub>, Li[BH<sub>4</sub>] or a mixture of MgCl<sub>2</sub>/Mg[HMDS]<sub>2</sub> (HMDS = hexamethyldisilazide) in THF. Quantum chemical calculations suggested the possibility of anion decomposition at the negative electrode, leading to an electronically insulating MgF<sub>2</sub> layer (rutile structure) on all the electrode materials tested. This hypothesis was confirmed by an XPS investigation of electrodes exposed to the electrolytes containing the WCAs  $[\text{Al}(\text{OR}^{\text{F}})_4]^-$  and  $[\text{Al}(\text{OC}(\text{H})(\text{CF}_3)_2)_4]^-$  at negative potentials, which only showed the presence of MgF<sub>2</sub> for the  $[\text{Al}(\text{OR}^{\text{F}})_4]^-$  electrolyte, but not for the related  $[\text{Al}(\text{OC}(\text{H})(\text{CF}_3)_2)_4]^-$  electrolyte (which allowed to deposit magnesium reversibly on the electrode).

## Introduction

An increasing energy demand as well as the implementation of renewable energy sources into the power grid require research progress in the field of energy storage. The low availability of lithium in the earth's crust and in seawater<sup>[1]</sup> as well as safety concerns drive researchers towards more abundant elements in their search for anode materials. Magnesium is 300 times more abundant than lithium, 24 times cheaper and can be employed as a safe negative metal electrode due to its dendrite-free metal deposition and non-pyroscopic nature.<sup>[2]</sup> Mg shows a relatively low redox potential (Mg: -2.37 V vs. SHE, Li: -3.04 V vs. SHE)<sup>[3]</sup> and delivers a high volumetric capacity (Mg: 3832 mAh cm<sup>-3</sup>, Li: 2062 mAh cm<sup>-3</sup>).<sup>[4]</sup> However, its low redox potential makes the use of non-aqueous solvents mandatory,

most of which form a passivation layer on the metal surface. In contrast to lithium-ion batteries, this passivation layer is not Mg<sup>2+</sup>-ion conductive and disrupts the electrochemical reaction at the electrodes.<sup>[5]</sup> Only ethers, such as tetrahydrofuran and glymes, show a sufficient stability against Mg metal. Hence, reported changes of the electrolyte composition focused on the variation of the electrolyte salt.

Early Mg-battery electrolytes originated from Grignard reagents, which, due to their reductive and nucleophilic character, showed a low oxidative stability of less than 2 V and poor conductivity.<sup>[6]</sup> Following the work of Gregory and their reversible deposition from organoborates in ethereal solutions,<sup>[7]</sup> indicating the importance of the Lewis acid and transmetallation, the Aurbach group developed dichlorocomplex organoaluminate electrolytes (DCC) with a stability of up to 2.2 V vs. Mg, which was used for the first rechargeable magnesium battery prototype in the year 2000.<sup>[8]</sup> While being a breakthrough for Mg-batteries, this system could not rival lithium-ion batteries due to the low capacity of the Chevrel phase cathode and its low voltage.<sup>[9]</sup> Therefore, the development of high voltage electrolytes and cathodes is necessary for applications. To achieve this, the Aurbach group developed the all-phenyl complex electrolyte, effectively eliminating the decomposition pathway via β-H atoms and with an anodic stability of up to 3.2 V vs. Mg.<sup>[10]</sup> The combination with a high capacity sulfur cathode posed further problems due to the nucleophilicity of these electrolytes. To overcome this issue, a non-nucleophilic electrolyte combining [HMDS]MgCl and AlCl<sub>3</sub> was developed with improved cycling performance.<sup>[11]</sup> Due to the chloride content of all these electrolytes, heavy corrosion of

[a] A. Schmidt, H. Koger, A. Barthélémy, Prof. Dr. I. Krossing  
Institut für Anorganische und Analytische Chemie und Freiburger Materialforschungszentrum (FMF)  
Universität Freiburg  
Albertstr. 21, 79104 Freiburg, Germany  
E-mail: krossing@uni-freiburg.de

[b] G. Studer, Prof. Dr. B. Esser  
Institute for Organic Chemistry II and Advanced Materials  
Ulm University  
Albert-Einstein-Allee 11, 89081 Ulm, Germany

 Supporting information for this article is available on the WWW under <https://doi.org/10.1002/batt.202200340>

 © 2022 The Authors. *Batteries & Supercaps* published by Wiley-VCH GmbH. This is an open access article under the terms of the Creative Commons Attribution Non-Commercial License, which permits use, distribution and reproduction in any medium, provided the original work is properly cited and is not used for commercial purposes.

battery components (e.g. current collectors) occurred, which moved chloride-free alternatives containing weakly coordinating anions (WCAs) (examples see Scheme 1), our long standing research interest,<sup>[12–16]</sup> into the focus of researchers. After preliminary work by Mohtadi using  $Mg[BH_4]_2$ ,<sup>[17]</sup> which, as a reducing agent, shows poor oxidative stability, boron-cluster anions and carborates were used as chloride-free electrolyte salts.<sup>[3,18]</sup> These borates, while showing a high stability, are poorly soluble in ethers, lowering the energy density. The work of the Lavallo group showed carborates in 0.75 M solutions of the Mg-carborate salt in tri- or tetraglyme.<sup>[19a,b,c]</sup> Their cation reduction approach for synthesis of Mg-carborates has since been adopted by other groups.<sup>[19a]</sup> Overall, weakly coordinating carborates seem like a good choice for Mg batteries, since there is almost no interface observed during Mg-plating.<sup>[19b]</sup> As alternatives to carborates, the groups of Zhao-Karger<sup>[4,20]</sup> and Arnold<sup>[21]</sup> synthesized  $[Mg(DME)_3][B(Ohfip)_4]_2$  and  $[Mg(DME)_n][Al(Ohfip)_4]_2$  ( $hfip = C(H)(CF_3)_2$ ), which show high solubility in DME and high Coulombic efficiencies for Mg plating and stripping. A high anodic stability of  $>4$  V and 3.5 V, respectively, was observed by both groups due to the addition of electron-withdrawing groups to the anion. The  $hfip$  electrolytes have been further investigated and other WCA-electrolytes have been developed and tested.<sup>[22,23,24]</sup>

We note that these borate and aluminate WCAs originate from Strauss's<sup>[25]</sup> and our group<sup>[12,26,27]</sup> and have been extensively used in diverse fields, i.e., for reactive cations<sup>[28]</sup> and ionic liquids,<sup>[15]</sup> but also battery electrolyte work.<sup>[13,29,30]</sup> The most chemically robust and least coordinating WCA of this entire WCA class is the one in which the remaining  $\beta$ -H atoms in the  $hfip$ -residue are replaced by  $CF_3$  groups to form the  $[Al(OR^F)_4]^-$  anion ( $R^F = C(CF_3)_3$ ). It was first introduced by our group in 2001,<sup>[12]</sup> heavily used for reactive cation work,<sup>[16,28]</sup> but, for example, we also analyzed the capacity of its  $[NR_4]^+$  salts to allow for electrochemistry in low polarity solvents.<sup>[27,31]</sup> Later, the groups of Lau<sup>[32]</sup> and Keyzer<sup>[33]</sup> synthesized  $[Mg(THF)_7][Al(OR^F)_4]_2$  and  $[Mg(THF)_6][Al(OR^F)_4]_2$  and demonstrated superior electrochemical properties for the salts. However, the synthetic routes to these electrolyte salts led to impurities, which are difficult to remove and can change the electrochemical behavior. First, there is the presence of THF as a ligand in the cation, which is strongly bound to magnesium and therefore remains in the electrolyte as an impurity, even if other solvents

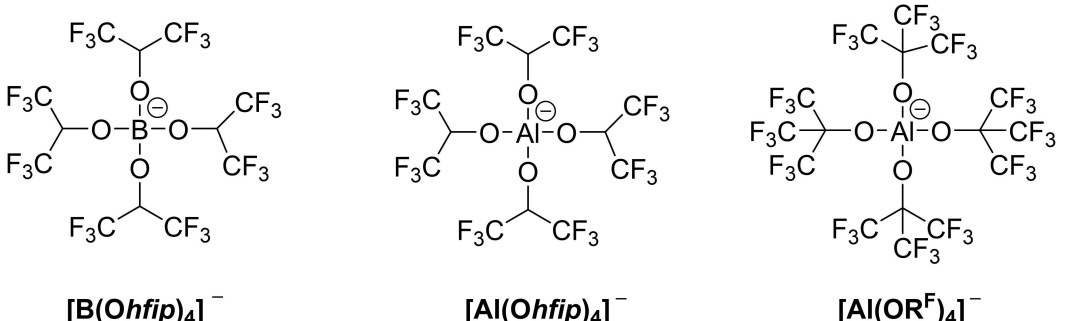
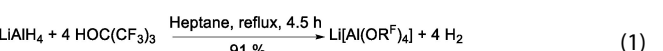
are used. Second, due to the synthetic routes chosen,  $LiCl$  or  $NaCl$  are produced as byproducts and cannot be removed completely from the electrolyte salt, rendering both electrolytes non-free from chloride.

Given the performance shown by these groups, we decided to investigate this system and develop a synthetic route using starting materials previously published by our group,<sup>[12,34]</sup> to yield a clean and chloride-free product. The synthesized salt should contain ligands/solvent molecules, which can be easily exchanged with other ligands unlike the THF-complexes. DME solutions of these pure salts were then investigated electrochemically regarding their electrolyte performance.

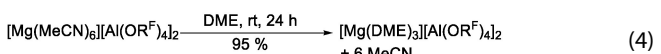
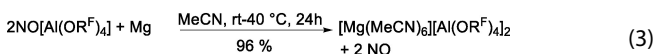
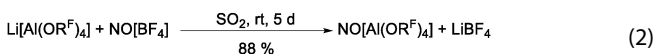
## Results and Discussion

### Synthesis and analysis of magnesium aluminates

The synthesis of  $[Mg(MeCN)_6][Al(OR^F)_4]_2$  was previously reported by our group as a product of a reaction, where  $[hexamethylbenzene][Al(OR^F)_4]$  and Mg were combined in *ortho*-difluorobenzene (*o*DFB) in the presence of small amounts of MeCN.<sup>[35]</sup> For electrochemical applications, it was synthesized here in three steps using easily accessible materials published by our group and in analogy to the synthesis of  $[Mg(MeCN)_6][PF_6]_2$  by Keyzer et al.<sup>[36]</sup> In the first step,  $Li[Al(OR^F)_4]$  is synthesized by alcoholysis of  $LiAlH_4$  with four equivalents of  $HOR^F$  [Eq. (1)].<sup>[12,37]</sup> The  $Li^+$  cation is then exchanged by metathesis<sup>[34]</sup> and stirring with  $NO[BF_4]$  in  $SO_2$ , forming soluble  $NO[Al(OR^F)_4]$  and insoluble  $Li[BF_4]$  [Eq. (2)].  $NO[Al(OR^F)_4]$  then allows the formation of contaminant-free  $[Mg(MeCN)_6][Al(OR^F)_4]_2$  by stirring and heating a MeCN solution of  $NO[Al(OR^F)_4]$  with an excess of Mg [Eq. (3)]. The gaseous side product NO escapes from the reaction, while the excess Mg can be removed by filtration, leaving  $[Mg(MeCN)_6][Al(OR^F)_4]_2$  as the only soluble ionic compound in the reaction mixture. Removing the solvent at inert conditions affords a colorless clean powder of  $[Mg(MeCN)_6][Al(OR^F)_4]_2$ . MeCN as a ligand may be exchanged for oxygen donor ligands due to the oxophilic nature of  $Mg^{2+}$ . Here, the ligands were exchanged for DME, as it is the common electrolyte solvent for Mg-batteries [Eq. (4)].



Scheme 1. Structures of the  $[B(Ohfip)_4]^-$ ,  $[Al(Ohfip)_4]^-$  and  $[Al(OR^F)_4]^-$  anions.



The successful and quantitative metathesis in Equation (2) is evidenced by IR, Raman and NMR spectroscopy (full spectra are depicted in Figures S2–S6, Tables S3 and S4). Figure S2 shows the area of the  $[\text{NO}]^+$  and MeCN vibrational bands in the IR and Raman spectra.  $\text{NO}[\text{Al}(\text{OR}^{\text{F}}_4)_4]$  exhibits a single distinctive vibrational  $[\text{NO}]^+$ -band at  $2340 \text{ cm}^{-1}$  (Raman)/  $2338 \text{ cm}^{-1}$  (IR), which is absent after the reaction with Mg. Instead, two new bands appear at  $2296$  and  $2323 \text{ cm}^{-1}$  (Raman)/  $2295$  and  $2321 \text{ cm}^{-1}$  (IR), which are attributed to MeCN in octahedral coordination [Eq. (3)]. These CN-stretches vanish after stirring a solution of  $[\text{Mg}(\text{MeCN})_6][\text{Al}(\text{OR}^{\text{F}}_4)_4]_2$  in DME and removal of the solvent *in vacuo* [Eq. (4)]. All bands observed by vibrational spectroscopy are in accordance with known or calculated spectra and can be assigned either to  $[\text{NO}]^+$ , the coordinated MeCN and DME ligands or the  $[\text{Al}(\text{OR}^{\text{F}}_4)_4]^-$  anion (Tables S3 and S4). NMR spectroscopy allowed to further investigate the purity of the electrolyte salts. Using oDFB as, or adding oDFB to the solvent allowed the quantification of the ligand/anion ratio by the integration ratio of the anion and oDFB fluorine signals as well as the integration ratio of ligand and oDFB hydrogen signals. The NMR spectra of  $[\text{Mg}(\text{MeCN})_6][\text{Al}(\text{OR}^{\text{F}}_4)_4]_2$  in DME (Figure S7) show a pristine, quasi impurity-free spectrum. The main signals at  $3.27$  and  $3.44 \text{ ppm}$  are assigned to DME, to which the spectrum was calibrated. The multiplet at  $7.24 \text{ ppm}$  in the  $^1\text{H}$  NMR spectrum belongs to oDFB, while the singlet at  $1.94 \text{ ppm}$  is assigned to MeCN. The tiny singlet at  $0.09 \text{ ppm}$  can be assigned to silicon grease from the joint, while the tiny triplet at  $0.13 \text{ ppm}$  belongs to an unidentified impurity, possibly a cyclic dimethylsiloxane formed by reaction of  $[\text{Mg}(\text{MeCN})_6][\text{Al}(\text{OR}^{\text{F}}_4)_4]_2$  with silicon grease. In the  $^{19}\text{F}$  NMR spectrum, only two signals were observed, assigned to oDFB at  $-140.5 \text{ ppm}$  and the  $[\text{Al}(\text{OR}^{\text{F}}_4)_4]^-$  anion at  $-75.9 \text{ ppm}$ . After integration, the ratio between MeCN and  $[\text{Al}(\text{OR}^{\text{F}}_4)_4]^-$  was calculated to be  $6.00:2.00$ , confirming the successful synthesis of the desired salt.

The same procedure was conducted with  $[\text{Mg}(\text{DME})_3][\text{Al}(\text{OR}^{\text{F}}_4)_4]_2$  except for a change in solvent. Since quantification of the DME ligand cannot be performed in DME as solvent, the  $^1\text{H}$  and  $^{19}\text{F}$  NMR spectra were collected from a solution in pure oDFB (Figure S8). The  $^1\text{H}$  NMR spectrum was calibrated to oDFB at  $6.96 \text{ ppm}$ . The remaining peaks were assigned to silicon grease at  $0.26 \text{ ppm}$ , and ( $\text{Mg}^{2+}$ -coordinated, downfield shifted) DME at  $4.06$  and  $4.33 \text{ ppm}$ . The fact that the most intense impurity signal is smaller than the  $^{13}\text{C}$  satellites of DME again underlines the high purity of the obtained product. The  $^{19}\text{F}$  NMR spectrum shows no signals other than those of oDFB at  $-139.5 \text{ ppm}$  and the  $[\text{Al}(\text{OR}^{\text{F}}_4)_4]^-$  anion at  $-75.4 \text{ ppm}$ . The calculation of the ligand-to-anion ratio was conducted in analogy to the MeCN-complex. The anion/ligand ratio was determined to be  $2.00:3.00$ , and therefore we conclude that the desired complex was successfully obtained. Careful analysis of this electrolyte salt by  $^1\text{H}$  NMR spectroscopy gave no signal that can be assigned to water. Hence, given that the largest impurity signal was integrated to  $10 \text{ ppm}$  and assuming it would be water, we expect a similar or even lower water content for the electrolyte, given that completely anhydrous DME was used for electrolyte preparation.

Crystals of  $[\text{Mg}(\text{MeCN})_6][\text{Al}(\text{OR}^{\text{F}}_4)_4]_2$  were obtained from a concentrated solution of the electrolyte salt in MeCN at  $-31^\circ\text{C}$ , while  $[\text{Mg}(\text{DME})_3][\text{Al}(\text{OR}^{\text{F}}_4)_4]_2$  was crystallized by layering a DME solution of the electrolyte with *n*-pentane. The molecular structures of the complex cations of both salts obtained by single-crystal X-ray diffraction (scXRD) are shown in Figure 1. In addition, the phase purity of both bulk compounds was confirmed by powder X-ray diffraction (pXRD) of the respective bulk microcrystalline products. The simulated diffractograms from the single-crystal data are in very good agreement with the pXRD-data for both complexes (Figures S11 and S12).

The comparatively poor qualities of the refinement models do not allow to discuss structural parameters (for  $[\text{Mg}(\text{MeCN})_6][\text{Al}(\text{OR}^{\text{F}}_4)_4]_2$ )

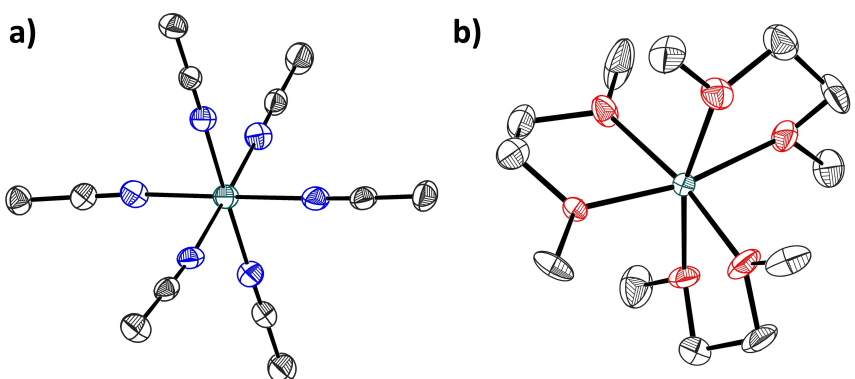


**Figure 1.** Molecular structure of a) the  $[\text{Mg}(\text{MeCN})_6]^{2+}$  cation and b) the  $[\text{Mg}(\text{DME})_3]^{2+}$  cation in the  $[\text{Al}(\text{OR}^{\text{F}}_4)_4]^-$  salts (cyan: magnesium; black: carbon; blue: nitrogen; red: oxygen). Thermal ellipsoids are shown at the 50 % probability level, hydrogen atoms and anions were omitted for clarity.

$[\text{Al}(\text{OR}^{\text{F}}_4)_4]_2$ :  $R_1 = 0.1380$ ,  $wR_2 = 0.4566$ ; for  $[\text{Mg}(\text{DME})_3][\text{Al}(\text{OR}^{\text{F}}_4)_4]_2$ :  $R_1 = 0.0845$ ,  $wR_2 = 0.2352$ ). However, the depicted molecular structures secure the atomic connectivities and allow to examine the phase purity by powder XRD. Full data on the status of the refinement is included in the SI (Table S5). In both structures, the MeCN and DME molecules are coordinated in octahedral fashion around the  $\text{Mg}^{2+}$  center. We expected that DME, forming a favorable chelate, should be thermodynamically advantageous to expel the MeCN ligand from the complex. To our surprise, quantum chemical calculations using the 'gold standard' method CCSD(T) with a large quadruple zeta basis set suggest that the exchange of the N-ligand with the O-ligand is **not** the driving force for this reaction ( $\Delta_r H^\circ = +149 \text{ kJ mol}^{-1}$ ). Furthermore, the chelate effect, release of six MeCN molecules after DME coordination and the resulting increase in entropy are also **not** enough to drive the reaction towards the formation of a  $[\text{Mg}(\text{DME})_3]^{2+}$ -complex ( $\Delta_r G^\circ = +105 \text{ kJ mol}^{-1}$ ). Finally, only the beneficial solvation of the  $[\text{Mg}(\text{DME})_3]^{2+}$ -cation in DME allows for the reaction to proceed ( $\Delta_r G^\circ = -49 \text{ kJ mol}^{-1}$ , Scheme 2).

### Electrochemical investigation of $[\text{Mg}(\text{MeCN})_6][\text{Al}(\text{OR}^{\text{F}}_4)_4]_2$ and $[\text{Mg}(\text{DME})_3][\text{Al}(\text{OR}^{\text{F}}_4)_4]_2$

Having established the purity of the synthesized aluminates, the electrochemical properties of their 0.2 M electrolyte solutions were investigated.

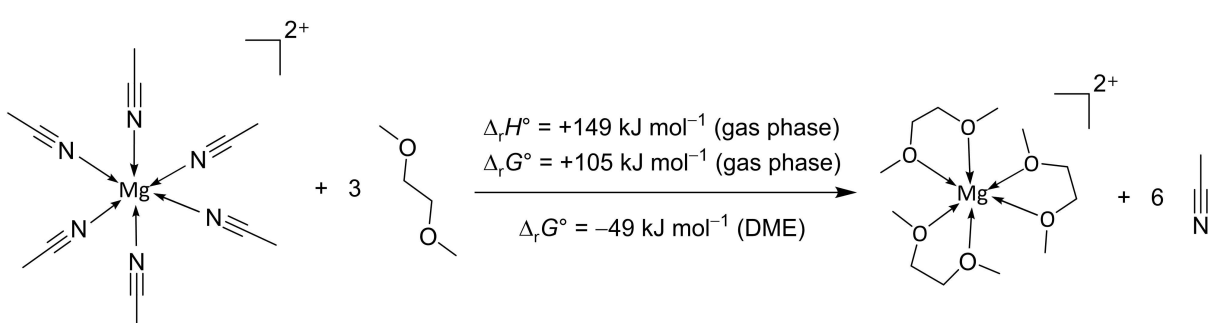
**Cyclic and linear sweep voltammetry in DME solution:** Since no electrochemical activity was observed in MeCN (Figure S13), the anodic stability of the electrolyte was investigated in DME as a typical magnesium electrolyte solvent by using linear sweep voltammetry (LSV). Since Keyzer et al. reported superior oxidative stability at Pt and Au electrodes<sup>[33]</sup> and Zhao-Karger et al. demonstrated slightly lower overpotentials on Cu electrodes for magnesium deposition from  $\text{Mg}[\text{B}(\text{Ohf})_4]_2$  electrolytes,<sup>[20]</sup> these three electrode materials were chosen for the LSV investigation. But first, the electrochemical solvent window of DME was determined by CV using  $[\text{NBu}_4][\text{Al}(\text{OR}^{\text{F}}_4)_4]$  as a conducting salt (Figure 3 left). It shows a flat line between  $-1.3$  and  $+4.4$  V vs.  $\text{Mg}^{2+}/\text{Mg}$ , demonstrating the quality of the WCA in the electrolyte, i.e., the purity of the

solvent and salt used for the electrolytes. Importantly, it shows no increase in current between  $-1$  and  $+1$  V vs.  $\text{Mg}^{2+}/\text{Mg}$  as the intended measuring window for magnesium deposition.

The LSV in Figure 2 on the right, shows great oxidative stability of the electrolyte against a Mg reference at a Pt and Au working electrode. At both electrodes the onset of the oxidative decomposition is at 3.5 V vs.  $\text{Mg}^{2+}/\text{Mg}$  at the Au electrode and at 3.7 V vs.  $\text{Mg}^{2+}/\text{Mg}$  at Pt, while the Cu electrode shows an increase in current at 2.3 V, possibly due to copper dissolution at said potential. Therefore, the cyclic voltammetry conditions should be chosen accordingly, to prevent Cu oxidation. Note that our oxidative onset potentials on our electrodes are shifted by ca.  $+0.5$  V towards higher potentials compared to the experiments of Keyzer.<sup>[33]</sup> Furthermore, our experiments show a linear increase in current, while the literature<sup>[33]</sup> shows curvatures even in the supposedly "Cl<sup>-</sup>" free" electrolyte (Figure S14), underlining the influence of even low chloride amounts on the electrolyte properties and the oxidative onset potential.

**Mg-deposition in DME solution:** With the above background, the apparently favorable properties of the WCA  $[\text{Al}(\text{OR}^{\text{F}}_4)_4]^-$  for electrolytes and the improved oxidative stability of the  $[\text{Mg}(\text{DME})_3][\text{Al}(\text{OR}^{\text{F}}_4)_4]_2$  electrolyte salt in DME compared to previously published results, the deposition and stripping of Mg from the DME complex was investigated using cyclic voltammetry. Hence, a 0.2 M solution of  $[\text{Mg}(\text{DME})_3][\text{Al}(\text{OR}^{\text{F}}_4)_4]_2$  in DME was examined in the range between  $+1$  and  $-1$  V vs.  $\text{Mg}^{2+}/\text{Mg}$  using a Pt or Cu working electrode and freshly polished Mg-ribbons as counter- and reference electrodes (Figure 3). We note that in this range of the CV curve, a 0.2 M solution of  $[\text{NBu}_4][\text{Al}(\text{OR}^{\text{F}}_4)_4]$  in DME shows a flat line (Figure 2 left).

Surprisingly, the overall current during this experiment is low, showing no indication of a metal deposition or dissolution. This is not in accordance with the literature.<sup>[32,33]</sup> It is noticeable, that the current decreases with every cycle of the experiment from  $0.738 \text{ mA cm}^{-2}$  to  $0.365 \text{ mA cm}^{-2}$  in cycle 10, which might hint at a passivating reaction at the electrodes. Further experiments with scan rates of 50, 20, 10 and  $5 \text{ mVs}^{-1}$  showed no change in electrochemical activity (see Figure S19). A similar experiment with 0.2 M  $[\text{Mg}(\text{DME})_3][\text{Al}(\text{OR}^{\text{F}}_4)_4]_2$  in pure THF as



**Scheme 2.** Reaction enthalpy ( $\Delta_r H^\circ$ ) and standard Gibbs energy ( $\Delta_r G^\circ$ ) for the ligand exchange of MeCN to DME in the gas phase and in DME solution at 298 K ( $\epsilon_r = 7.30$ ,<sup>[1]</sup> DLPNO-CCSD(T)/cc-pVQZ single point energies on RI-B3LYP(D3BJ)/def2-TZVPP optimized structures, solvation energies calculated with COSMO model at the RI-B3LYP(D3BJ)/def2-TZVPP level).

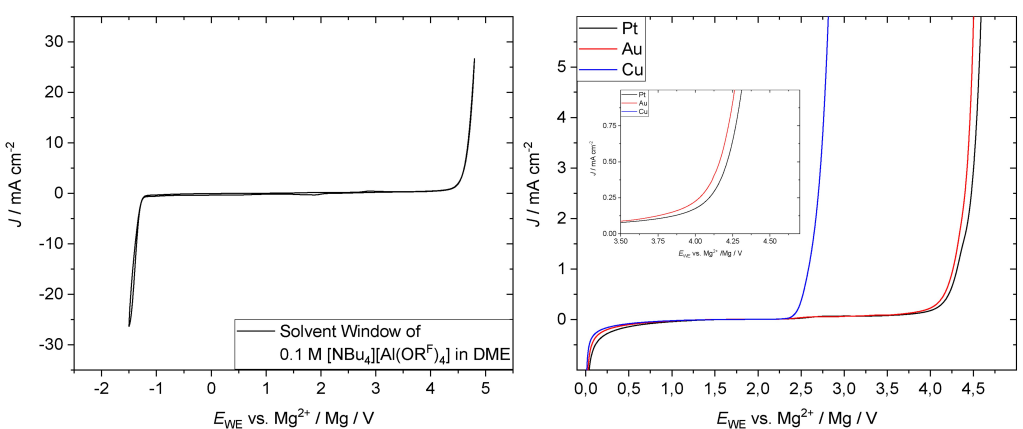


**Figure 2.** Cyclic voltammogram (cycle 2) of the electrochemical solvent window of a 0.1 M solution of  $[NBu_4][Al(OR^F)_4]$  in DME at a scan rate of  $100 \text{ mV s}^{-1}$  on a Pt electrode (left). LSV experiment of a 0.2 M solution of  $[Mg(DME)_3][Al(OR^F)_4]_2$  in DME with Au, Cu and Pt-working electrode (right). The inset shows the onset of oxidation at Pt and Au electrodes for the electrolyte.

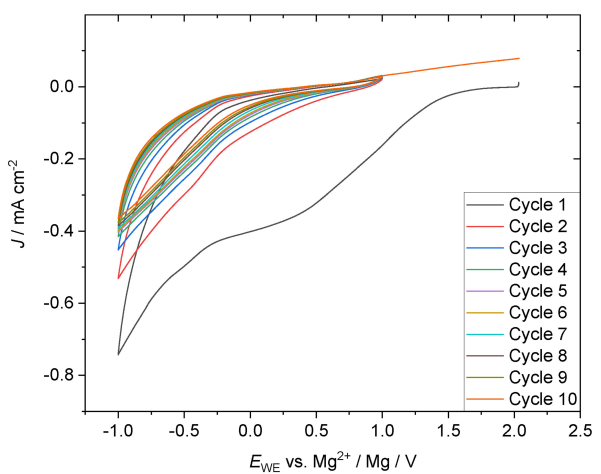


**Figure 3.** Cyclic voltammogram of a 0.2 M solution of  $[Mg(DME)_3][Al(OR^F)_4]_2$  in DME at a scan rate of  $100 \text{ mV s}^{-1}$  using a Pt working electrode.

solvent at scan rates of 100 and  $5 \text{ mV s}^{-1}$  showed no electrochemical activity.

Since no electrochemical activity was observed in the experiments with pristine electrolyte, 10 mol% of additives were included in the electrolyte and the resulting solutions were electrochemically investigated between  $-1$  and  $+1$  V vs.  $Mg^{2+}/Mg$ . We decided to add substances that were part of functioning electrolytes or the electrolyte salts themselves. This could have beneficial effects on the deposition complexes or the interphase. The literature examples<sup>[32,33]</sup> contained  $Cl^-$  and THF as contaminants. Hence,  $Cl^-$ -salts ( $LiCl$ ,  $NaCl$ ,  $MgCl_2$ ) were utilized as additives. Furthermore,  $Li[BH_4]$  and a mixture of  $MgCl_2/Mg[HMDS]_2$  ( $HMDS =$  hexamethyldisilazide)<sup>[38]</sup> in THF was added, since deposition and stripping from both these mixture and from  $[BH_4]^-$ -electrolytes<sup>[17]</sup> have been described in the literature (Figure 4). THF (20  $\mu\text{L}$ ) was added to each additivated electrolyte, if no electrochemical reaction was observed in THF-free CV experiments, and the experiments were rerun (Figure 4 right).

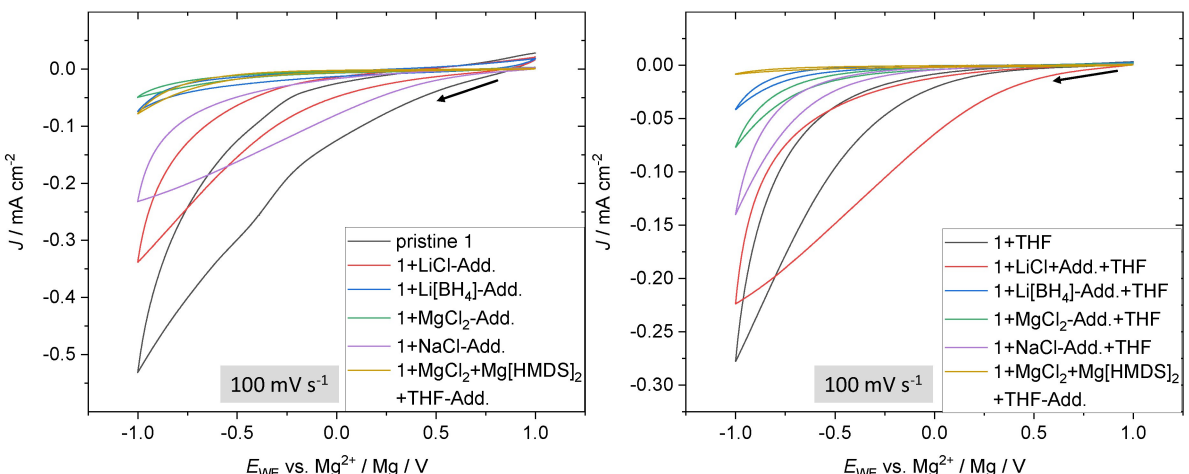


**Figure 4.** Cyclic voltammograms of a 0.2 M solution of  $[Mg(DME)_3][Al(OR^F)_4]_2$  (1) including no (pristine) or 10 mol% additives in DME at a scan rate of  $100 \text{ mV s}^{-1}$  using a Pt working electrode (left). The experiments were repeated with an additional 20  $\mu\text{L}$  of THF added to the electrolyte used for the measurement on the left, all at a scan rate of  $100 \text{ mV s}^{-1}$  and using a Pt working electrode (right). The second cycle of all experiments is shown.

All experiments showed low current densities regardless of the employed additive. The pristine electrolyte showed the highest current density ( $0.53 \text{ mA cm}^{-2}$ ), followed by the electrolytes with added LiCl and NaCl. 10 mol% MgCl<sub>2</sub> were not fully soluble in DME and displayed the lowest current of the investigated additivated electrolytes ( $0.05 \text{ mA cm}^{-2}$ ). The electrolytes with additional Li[BH<sub>4</sub>] ( $0.07 \text{ mA cm}^{-2}$ ) and a mixture of MgCl<sub>2</sub>/Mg[HMDS]<sub>2</sub> ( $0.08 \text{ mA cm}^{-2}$ ) showed very low current densities and no electrochemical activity. None of the investigated additives exhibits a beneficial effect towards a Mg deposition. The addition of THF to each electrolyte only led to a decrease in current density for every electrolyte, and no change in electrochemical activity was observed. To exclude a kinetic effect, the measurements were repeated with the same solutions at a scan rate of  $5 \text{ mV s}^{-1}$  (Figure S16). The effect of the electrode was also investigated by repeating the experiments using a Cu working electrode and scan rates of  $100 \text{ mV s}^{-1}$  (Figure S17) and  $5 \text{ mV s}^{-1}$  (Figure S18). It is obvious that none of the employed additives, electrodes or scan rates showed a positive effect towards Mg deposition, rendering the application of this electrolyte in a battery cell, as observed in

our experiments, impossible. It seems that the exact composition of impurities acting as additives, electrolyte salt and external conditions are necessary for a successful electrochemical application.

**Validation of Mg deposition and stripping:** To validate our setup for Mg deposition and stripping by CV, an electrolyte containing the salt [Mg(DME)<sub>3</sub>][Al(Ohfip)<sub>4</sub>]<sub>2</sub> in DME, as prepared independently in our group, was studied. A  $0.2 \text{ M}$  solution was investigated in analogy to the CV experiments with [Mg(DME)<sub>3</sub>][Al(OR<sup>F</sup>)<sub>4</sub>]<sub>2</sub> (Figure 5a). Furthermore, a more diluted,  $0.01 \text{ M}$  solution of [Mg(DME)<sub>3</sub>][Al(Ohfip)<sub>4</sub>]<sub>2</sub> in DME with  $0.1 \text{ M}$  [NBu<sub>4</sub>][Al(OR<sup>F</sup>)<sub>4</sub>]<sub>2</sub> as supporting electrolyte salt was tested (Figure 5b).

The CV of a pure and concentrated solution of [Mg(DME)<sub>3</sub>][Al(Ohfip)<sub>4</sub>]<sub>2</sub> shows the deposition of Mg with an overpotential of  $-715 \text{ mV}$  (Figure 5a). The current increases from this potential and returns to  $0 \text{ mA cm}^{-2}$  at  $-300 \text{ mV}$ , when the deposition process ends. The dissolution sets in at  $-143 \text{ mV}$  and reaches its peak current density at  $179 \text{ mV}$ . Not all deposited Mg was dissolved, since during the measurement pieces of deposited metal were observed to detach from the electrode. The diluted  $0.01 \text{ M}$  solution with an excess of

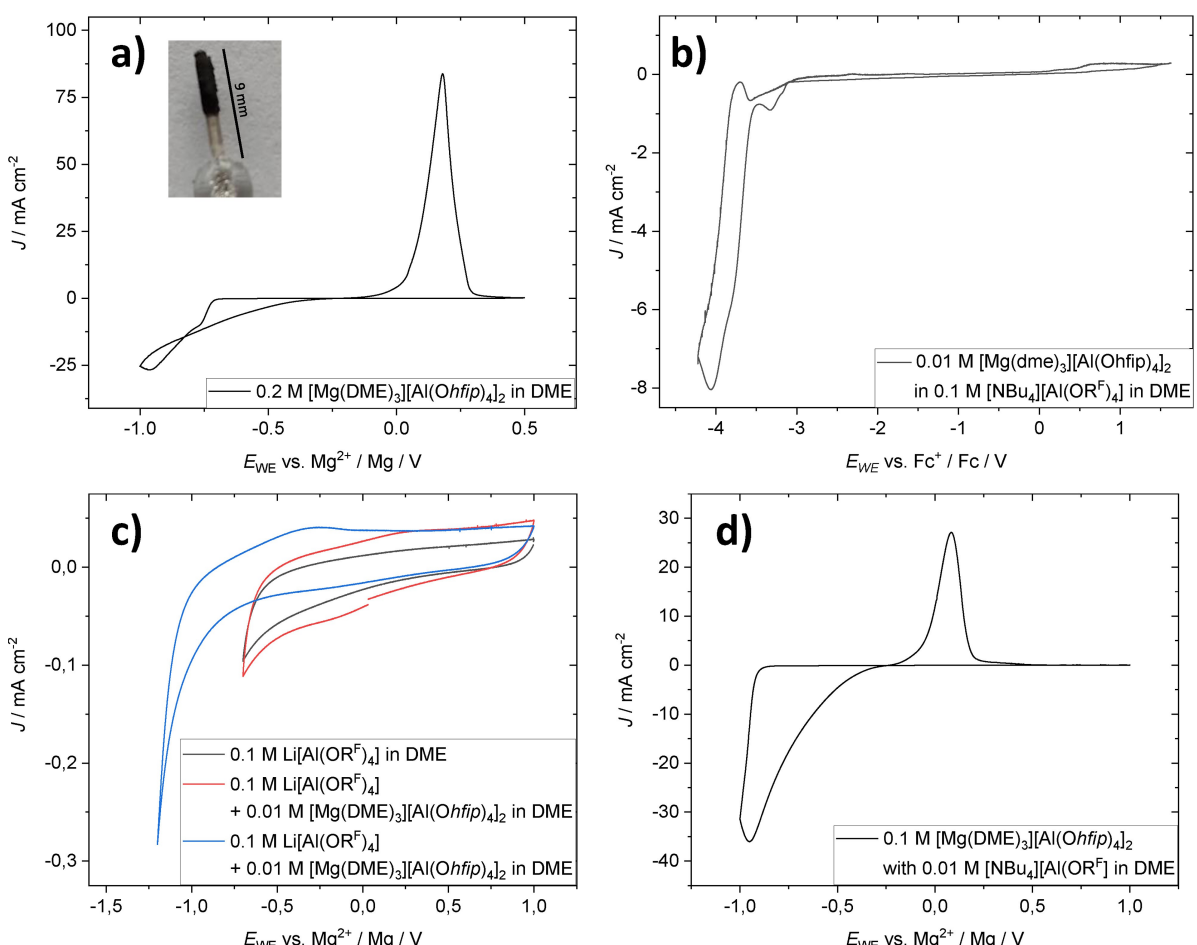


**Figure 5.** a) Cyclic voltammogram of a  $0.2 \text{ M}$  solution of [Mg(DME)<sub>3</sub>][Al(Ohfip)<sub>4</sub>]<sub>2</sub> in DME at  $100 \text{ mV s}^{-1}$  (cycle 2) using a Pt-electrode. Inset shows Mg deposition on a Pt wire from the same solution. b) Cyclic voltammogram of a  $0.01 \text{ M}$  solution of [Mg(DME)<sub>3</sub>][Al(Ohfip)<sub>4</sub>]<sub>2</sub> with  $0.1 \text{ M}$  [NBu<sub>4</sub>][Al(OR<sup>F</sup>)<sub>4</sub>]<sub>2</sub> in DME (cycle 2). c) Cyclic voltammogram of a  $0.1 \text{ M}$  solution of Li[Al(OR<sup>F</sup>)<sub>4</sub>] in DME at a sweep rate of  $100 \text{ mV s}^{-1}$  on a Pt electrode (black). After addition of  $0.01 \text{ M}$  [Mg(DME)<sub>3</sub>][Al(Ohfip)<sub>4</sub>]<sub>2</sub> the same potentials up to  $-0.7 \text{ V}$  (red) and  $-1.2 \text{ V}$  (blue) were scanned at  $100 \text{ mV s}^{-1}$  on a Pt-electrode. d) Cyclic voltammogram of  $0.1 \text{ M}$  [Mg(DME)<sub>3</sub>][Al(Ohfip)<sub>4</sub>]<sub>2</sub> with  $0.01 \text{ M}$  [NBu<sub>4</sub>][Al(OR<sup>F</sup>)<sub>4</sub>]<sub>2</sub> in DME at  $100 \text{ mV s}^{-1}$  (cycle 2) using a Pt-electrode.

$[\text{Al}(\text{OR}^{\text{F}})_4]^-$  conducting salt (0.1 M) in Figure 5b) shows no electrochemical activity. At  $-3.1 \text{ V}$  vs.  $\text{Fc}^+/\text{Fc}$ , a reductive current was observed, which could be attributed to either solvent decomposition or Mg deposition. Since no oxidative current was recorded, which would imply Mg dissolution, it is likely that the reductive current can be attributed to solvent decomposition. It seems that the presence of the  $[\text{Al}(\text{OR}^{\text{F}})_4]^-$  anion inhibits the deposition of Mg. Using  $\text{Li}[\text{Al}(\text{OR}^{\text{F}})_4]$  as an alternative to  $[\text{NBu}_4][\text{Al}(\text{OR}^{\text{F}})_4]$  as the supporting electrolyte salt, it was shown that this effect occurs independently from the cation of the conducting  $[\text{Al}(\text{OR}^{\text{F}})_4]^-$  electrolyte (Figure 5c). When reversing the concentrations of  $[\text{Al}(\text{Ohfip})_4]^-$  (0.1 M) and  $[\text{Al}(\text{OR}^{\text{F}})_4]^-$  (0.01 M), a high reductive and oxidative current was measured. The overpotentials for Mg deposition increased slightly to  $-876 \text{ mV}$ , while the dissolution occurs at  $-65 \text{ mV}$ , when including 0.01 M  $[\text{NBu}_4][\text{Al}(\text{OR}^{\text{F}})_4]_2$  in DME (Figure 5d). When employing  $\text{Li}[\text{Al}(\text{OR}^{\text{F}})_4]$  with an excess  $[\text{Mg}(\text{DME})_3][\text{Al}(\text{Ohfip})_4]_2$ , the same reactions can be observed (see Figure S25). Therefore, a deposition and dissolution of magnesium is only hindered if an excess of  $[\text{Al}(\text{OR}^{\text{F}})_4]^-$  is present.

#### Possible reasons for the suppressed Mg deposition in $[\text{Mg}(\text{DME})_3][\text{Al}(\text{OR}^{\text{F}})_4]_2$ electrolytes

Even though the weaker coordination of the  $[\text{Al}(\text{OR}^{\text{F}})_4]^-$  anion to  $\text{Mg}^{2+}$  and hence decreased ion-pairing should in theory lead to better electrochemical results than for  $[\text{Al}(\text{Ohfip})_4]^-$ , our findings cannot confirm this hypothesis or the results of the groups around Keyzer<sup>[33]</sup> and Lau.<sup>[32]</sup> To gain further insight into Mg deposition, quantum chemical calculations were conducted.

First, we studied the two cationic complexes synthesized in the process. For the possibility of Mg deposition, the  $\text{Mg}^{2+}$  center should significantly contribute to low-lying, unoccupied molecular orbitals of the complex (MOs). Therefore, the energies of the four lowest lying unoccupied MOs were calculated and presented graphically (Figure S30). The calculations show no significant coefficient on  $\text{Mg}^{2+}$  in the MeCN-complex, which agrees with the futile Mg deposition during the CV in MeCN. By contrast, the central  $\text{Mg}^{2+}$  ion contributes somewhat to the LUMO ( $-6.14 \text{ eV}$ ) and LUMO + 1 ( $-5.38 \text{ eV}$ ) in the DME complex. This should allow for the deposition of Mg from  $[\text{Mg}(\text{DME})_3][\text{Al}(\text{Ohfip})_4]_2$ , but does not explain the absence of the Mg deposition in the presence of an excess of  $[\text{Al}(\text{OR}^{\text{F}})_4]^-$ .

Yet, the reduction at the perfluorinated WCA surface of the  $[\text{Al}(\text{OR}^{\text{F}})_4]^-$  anion seemed likely to occur in the vicinity of a Mg surface. Therefore, the frontier MO energies were calculated and the coefficients are presented in Figure S31. For a reduction reaction, electrons have to be transferred from the electrode into the LUMO ( $+3.36 \text{ eV}$ ) of the anion. The energy levels of the three WCAs, i.e.,  $[\text{Al}(\text{OR}^{\text{F}})_4]^-$ ,  $[\text{Al}(\text{Ohfip})_4]^-$  and  $[\text{B}(\text{Ohfip})_4]^-$  are compared in Table 1, in addition to the Gibbs reaction energy of the one-electron reduction of the three WCAs according to Equation (5).

**Table 1.** Gibbs free energy for the one-electron reduction of three WCAs in DME ( $\varepsilon_r = 7.30$ )<sup>[1]</sup> according to Equation (5) and energy levels of the LUMOs for these WCAs, which should accept the incoming electron (RI-B3LYP(D3BJ)/def2-TZVPP).

| WCA                                     | $\Delta_r G^\circ(\text{Eq. 5}) [\text{kJ mol}^{-1}]$ | LUMO energy level of the WCA [eV] |
|---|---|-----------------------------------|
| $[\text{Al}(\text{OR}^{\text{F}})_4]^-$ | -53   | +3.36                             |
| $[\text{Al}(\text{Ohfip})_4]^-$         | +44   | +3.42                             |
| $[\text{B}(\text{Ohfip})_4]^-$          | -48   | +4.17                             |

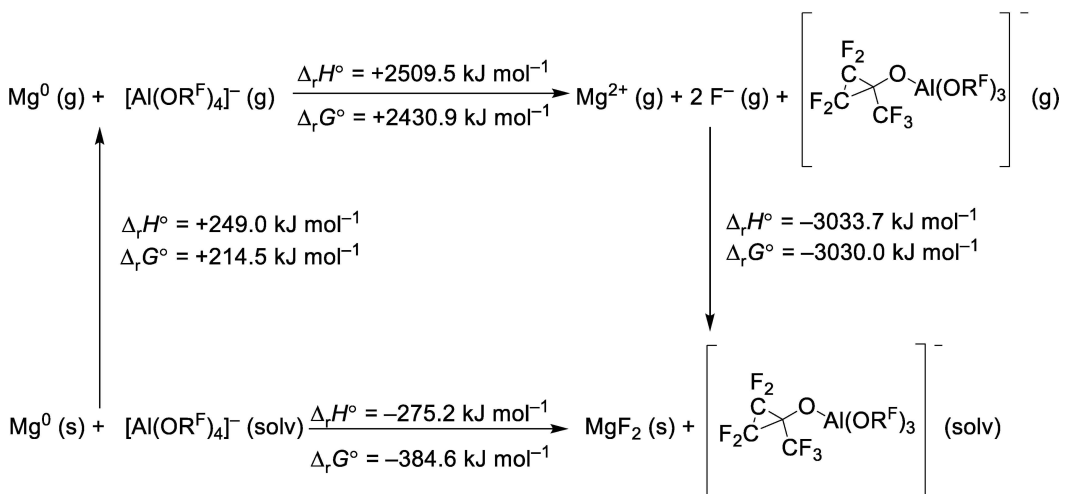


It follows from the values in Table 1 that the reduction of  $[\text{Al}(\text{Ohfip})_4]^-$  in DME is endergonic and thus thermodynamically unfavorable in solution, while the reduction of  $[\text{Al}(\text{OR}^{\text{F}})_4]^-$  and  $[\text{B}(\text{Ohfip})_4]^-$  is feasible in solution. However, the  $[\text{Al}(\text{OR}^{\text{F}})_4]^-$  anion has the lowest lying LUMO energy, implying that this anion is most prone to reduction by elemental Mg. The  $[\text{B}(\text{Ohfip})_4]^-$  anion has the highest lying LUMO, implying that the reduction of this anion may be kinetically hindered by the 0.8 eV higher LUMO level compared to  $[\text{Al}(\text{OR}^{\text{F}})_4]^-$ . However, the formation of small amounts of  $\text{MgF}_2$  from  $\text{Mg}[\text{B}(\text{Ohfip})_4]_2$  was confirmed in the literature.<sup>[24]</sup> In agreement with these considerations, Mg deposition was hitherto observed with electrolytes containing the WCAs  $[\text{Al}(\text{Ohfip})_4]^-$ <sup>[21]</sup> and  $[\text{B}(\text{Ohfip})_4]^-$ .<sup>[4,20]</sup>

If a thin layer of elemental Mg is deposited on the electrode, the reactive Mg – additionally polarized to negative potential at the electrode – could decompose the  $[\text{Al}(\text{OR}^{\text{F}})_4]^-$  anion and, more importantly, form a thin layer of heavily insulating  $\text{MgF}_2$ , which adopts the chemically very robust rutile structure. Scheme 3 delineates a calculated viable route to  $\text{MgF}_2$  from magnesium and the  $[\text{Al}(\text{OR}^{\text{F}})_4]^-$  anion.

The estimated thermodynamics of this postulated reaction from the Born-Haber cycle in Scheme 3 are in favor of  $\text{MgF}_2$  formation. Additionally,  $\text{MgF}_2$  leaves the reaction as an insulating colorless solid, favoring the reaction. The declining current density and lack of electrochemical activity combined with the thermodynamically possible anion decomposition at elemental Mg lead to our conclusion that passivation by  $\text{MgF}_2$  is likely occurring at the electrode surface. This hypothesis was investigated by XPS in the next section.

**Investigating the electrode surfaces by XPS:** The electrode surface was investigated by X-Ray photoelectron spectroscopy (XPS), which, according to our hypothesis, should include a thin layer of  $\text{MgF}_2$  on top of a Pt electrode, if a  $[\text{Al}(\text{OR}^{\text{F}})_4]^-$  electrolyte is used, but not if a  $[\text{Mg}(\text{DME})_3][\text{Al}(\text{Ohfip})_4]_2$  electrolyte is used. The attempt of Mg deposition with 0.2 M  $[\text{Mg}(\text{DME})_3][\text{Al}(\text{OR}^{\text{F}})_4]_2$  at constant current ( $-240 \mu\text{A}$ ) led to a rapid increase in potential (Figure S26). After 1 min the potential increased to  $-4.3 \text{ V}$  and to  $-8.2 \text{ V}$  after 4 min. At these potentials, the decomposition of the electrolyte solvent is likely, therefore an alternative way of Mg deposition was chosen. In CV experiments, the potential, at which the negative current increases, was identified to  $-3.2 \text{ V}$  (Figure S27). At this potential, Mg deposition was attempted by chronoamperometry for 2 h (Figure S28). During these 2 h no gas evolution was observed



**Scheme 3.** Calculated Born-Haber cycle for the reduction of  $[\text{Al}(\text{OR}^{\text{F}})_4]^-$  at a  $\text{Mg}^0$  surface in DME, yielding  $\text{MgF}_2$  and a perfluorinated alkoxyaluminate with a cyclopropane moiety (RI-B3LYP(D3BJ)/def2-TZVPP) ( $\epsilon_r = 7.30$ ).<sup>[1]</sup>

from the electrodes. A similar experiment was performed with  $[\text{Mg}(\text{DME})_3][\text{Al}(\text{O}^{\text{H}fip})_4]_2$  at a potential of  $-0.7 \text{ V}$  vs.  $\text{Mg}^{2+}/\text{Mg}$  for 2 h. Again, the optical difference was a thick, visible grey deposition on the Pt piece taken from the  $[\text{Mg}(\text{DME})_3][\text{Al}(\text{O}^{\text{H}fip})_4]_2$  electrolyte and an optically clean Pt piece taken from the  $[\text{Mg}(\text{DME})_3][\text{Al}(\text{OR}^{\text{F}})_4]_2$  electrolyte. To investigate our hypothesis, the depositions on these Pt pieces were compared with XPS measurements of pure  $\text{MgF}_2$  powder. The XPS binding energy was calibrated using the C1s signal of the internal adventitious carbon contamination (AdC), which has a variability of  $\pm 0.3 \text{ eV}$  due to its surface structure. For our case 284.8 eV was chosen (Figure S29).<sup>[39]</sup>

The Mg XPS spectra of  $\text{MgF}_2$  powder and the Pt-wire taken from the  $[\text{Mg}(\text{DME})_3][\text{Al}(\text{OR}^{\text{F}})_4]_2$  are in good accordance with each other. In the Mg 2 s spectrum (Figure 6 left),  $\text{MgF}_2$  shows a peak at 88.85 eV. The Pt-wire taken from the  $[\text{Al}(\text{OR}^{\text{F}})_4]^-$ -electrolyte shows a peak at 88.9 eV, while the Pt piece taken from the  $[\text{Al}(\text{O}^{\text{H}fip})_4]^-$ -electrolyte is shifted towards higher binding energy with a maximum at 90.65 eV. The Mg 2 p spectrum (Figure 6 middle) of the  $[\text{Al}(\text{OR}^{\text{F}})_4]^-$ -electrolyte shows a peak at 50.5 eV, which matches the peak of  $\text{MgF}_2$  at 50.45 eV.

These two spectra strongly suggest that  $\text{MgF}_2$  was formed from  $[\text{Mg}(\text{DME})_3][\text{Al}(\text{OR}^{\text{F}})_4]_2$ . Even though a metallic deposition could be visually observed from the  $[\text{Al}(\text{O}^{\text{H}fip})_4]^-$ -electrolyte, no  $\text{Mg}^0$  peak was observed. The absence of a  $\text{Mg}^0$  peak could be explained by a layer of electrolyte salt on top of the fluffy Mg-deposition on Pt, which shields the underlying Mg from the highly surface-sensitive X-rays. Note that the diameter of the WCA  $[\text{Al}(\text{O}^{\text{H}fip})_4]^-$  exceeds 1 nm, and already an electrolyte double layer might be sufficient to shield the elemental Mg from the X-rays during the XPS experiment.

Further hints towards the formation of  $\text{MgF}_2$  from  $[\text{Al}(\text{OR}^{\text{F}})_4]^-$ , but not from  $[\text{Al}(\text{O}^{\text{H}fip})_4]^-$  electrolytes, can be found in the F 1s XPS spectra (Figure 6 right). The deposition from  $[\text{Mg}(\text{DME})_3][\text{Al}(\text{O}^{\text{H}fip})_4]_2$  electrolyte shows one intense peak at 689.15 eV and a shoulder with weak intensity at 686.05 eV. The  $[\text{Mg}(\text{DME})_3][\text{Al}(\text{OR}^{\text{F}})_4]_2$  electrolyte shows two more distinct peaks, one of which is located at 689.15 eV, which could stem from the  $\text{CF}_3$  groups present in both anions. Another, less intense peak it found at 684.8 eV and is in good accordance with the  $\text{MgF}_2$  peak at 684.6 eV.

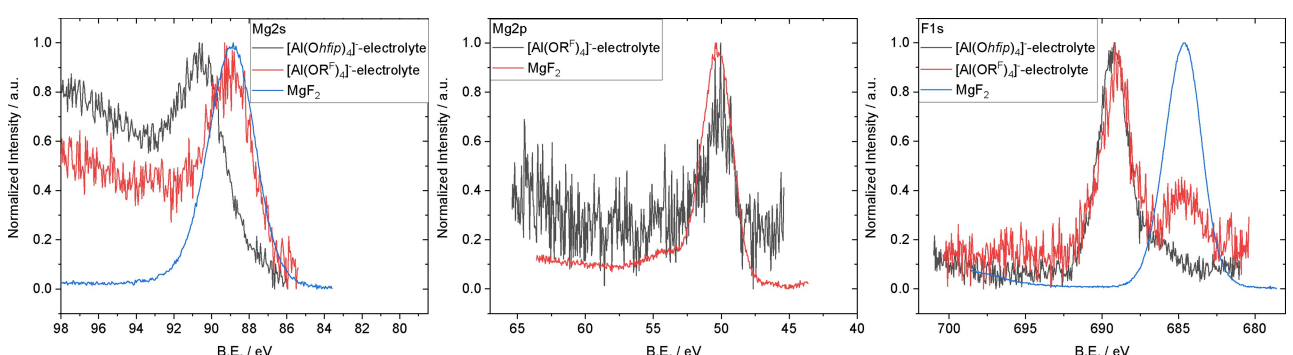


**Figure 6.** Mg 2 s XPS spectra of  $\text{MgF}_2$  and deposition from  $[\text{Mg}(\text{DME})_3][\text{Al}(\text{O}^{\text{H}fip})_4]_2$  and  $[\text{Mg}(\text{DME})_3][\text{Al}(\text{OR}^{\text{F}})_4]_2$  electrolytes (left) and Mg 2 p spectra of  $\text{MgF}_2$  and deposition from  $[\text{Mg}(\text{DME})_3][\text{Al}(\text{OR}^{\text{F}})_4]_2$  electrolyte (middle). F 1s XPS spectra of  $\text{MgF}_2$  and deposition from  $[\text{Mg}(\text{DME})_3][\text{Al}(\text{O}^{\text{H}fip})_4]_2$  and  $[\text{Mg}(\text{DME})_3][\text{Al}(\text{OR}^{\text{F}})_4]_2$  electrolytes (right). All spectra were calibrated with AdC and normalized to their peak with highest intensity (B.E. = Binding Energy).

The XPS spectra of Mg and F show strong hints that the  $[\text{Al}(\text{OR}^{\text{F}}_4)]^-$  anion decomposes at a fresh Mg electrode at negative potential to produce insulating  $\text{MgF}_2$ . This could explain the failure of our electrolyte to deposit Mg. What our experiments do not explain is the reported success in Mg deposition in the literature from magnesium electrolytes using  $[\text{Al}(\text{OR}^{\text{F}}_4)]^-$ .<sup>[32,33]</sup> The formation of  $\text{MgF}_2$  agrees with our calculations. Hence, both the  $[\text{B}(\text{Ohfip})_4]^-$  and  $[\text{Al}(\text{OR}^{\text{F}}_4)]^-$  anions are thermodynamically prone to reduction, while the  $[\text{Al}(\text{Ohfip})_4]^-$  anion is stable. Apparently, the high LUMO energy of  $[\text{B}(\text{Ohfip})_4]^-$  impedes reduction compared to the  $[\text{Al}(\text{OR}^{\text{F}}_4)]^-$  anion, leading to a much higher quantity of  $\text{MgF}_2$  formed from  $[\text{Al}(\text{OR}^{\text{F}}_4)]^-$  based electrolytes. The positive electrochemical results found in the literature seem to be due to a positive effect from contaminants found in these electrolytes, which could not be reproduced by incorporation of additives in our laboratory. Therefore, according to our results,  $[\text{Mg}(\text{DME})_3][\text{Al}(\text{OR}^{\text{F}}_4)_2]$  is the least favorable electrolyte salt of the compared salts.  $[\text{B}(\text{Ohfip})_4]^-$  is slightly more stable, while  $[\text{Al}(\text{Ohfip})_4]^-$  is supposed to be the most favorable of these anions.

## Conclusion

We herein investigated and characterized  $[\text{Mg}(\text{MeCN})_6][\text{Al}(\text{OR}^{\text{F}}_4)_2]$  and  $[\text{Mg}(\text{DME})_3][\text{Al}(\text{OR}^{\text{F}}_4)_2]$  as compounds that deemed promising for Mg battery applications. We demonstrated a new quantitative and straightforward route towards  $[\text{Mg}(\text{DME})_3][\text{Al}(\text{OR}^{\text{F}}_4)_2]$  which allows synthesizing the salt free of common contaminants, such as chloride. Vibrational spectroscopy, NMR spectroscopy, single crystal X-ray analysis as well as powder XRD verified the high purity of the synthesized compound. Crystal structures were obtained, revealing the respective molecular structures of the cations. The electrochemical behavior was investigated in MeCN and DME solvents, showing no electrochemical activity from either complex in these solvents on the tested Pt and Cu electrodes. The electrochemical activity was then investigated using common contaminants from previously published papers as additives. No electrochemical reactions were observed in CVs using these additives. Furthermore, the addition of an excess of the  $[\text{Al}(\text{OR}^{\text{F}}_4)]^-$  salt to a functioning electrolyte system, such as  $[\text{Mg}(\text{DME})_3][\text{Al}(\text{Ohfip})_4]_2$  in DME, shut down Mg electrodeposition, while smaller amounts only increased overpotentials of Mg-electrodeposition regardless of the counterion of the  $[\text{Al}(\text{OR}^{\text{F}}_4)]^-$  salt ( $[\text{NBu}_4]^+$  or  $\text{Li}^+$ ). The reason for an absence of electrochemical activity was examined using quantum chemical calculations. The formation of insulating  $\text{MgF}_2$  at the electrode through decomposition of the  $[\text{Al}(\text{OR}^{\text{F}}_4)]^-$  anion at a freshly deposited Mg surface or simply the pristine negative electrode as in eq. 5 was considered as a possibility. This hypothesis was investigated via XPS using Pt pieces, onto which a negative potential was applied for 2 h for Mg deposition. The comparison of the deposited material with  $\text{MgF}_2$  powder confirmed the presence of  $\text{MgF}_2$  on the Pt electrode after the deposition experiment, but only for the electrolyte with the  $[\text{Al}(\text{OR}^{\text{F}}_4)]^-$  salt, not for the one using the standard  $[\text{Mg}(\text{DME})_3][\text{Al}(\text{Ohfip})_4]_2$  salt

in DME. The formation of an insulating  $\text{MgF}_2$  layer would explain the lack of electrochemical activity in our experiments. This would also render further studies into this electrolyte not very promising.

Hence, we were rather surprised that in our hands multiple attempts to use  $[\text{Mg}(\text{DME})_3][\text{Al}(\text{OR}^{\text{F}}_4)_2]$  as an electrolyte salt for Mg-deposition and stripping were futile, although it contains our very best and least coordinating WCA compatible with many reactive environments. Instead and in agreement with the quantum chemical calculations collected in Table 1, we consider the WCA  $[\text{Al}(\text{Ohfip})_4]^-$  to be the superior choice for battery application.

In addition, all the results collected in this article point to the need to have a suitable stabilizing, magnesium ion conducting, but electronically insulating SEI layer also for magnesium batteries, else on the long run, no battery would work due to anion decomposition. To our knowledge, this important field of research is still in its infancies.<sup>[22,24,40]</sup>

Deposition Number(s) 2193348 (for  $[\text{Mg}(\text{DME})_3][\text{Al}(\text{OR}^{\text{F}}_4)_2]$ ) contain(s) the supplementary crystallographic data for this paper. These data are provided free of charge by the joint Cambridge Crystallographic Data Centre and Fachinformationszentrum Karlsruhe Access Structures service. Due to the rather poor quality of the refinement model for  $[\text{Mg}(\text{MeCN})_6][\text{Al}(\text{OR}^{\text{F}}_4)_2]$ , the structure was not uploaded into the CCDC.

## Acknowledgements

This work was supported by the Albert-Ludwigs-Universität Freiburg and by the DFG SPP2248 "Polymer-based Batteries" (project numbers 441215516 (BE) and 441215516 (IK)). This work contributes to the research performed at the FMF (Freiburg Materials Research Center), the FIT (Freiburg Center for Interactive Materials and Bioinspired Technologies), CELEST (Center for Electrochemical Energy Storage Ulm-Karlsruhe) and was funded by the German Research Foundation (DFG) under Project ID 390874152 (POLiS Cluster of Excellence, EXC 2154) as well as Project ID 390951807 (livMatS Cluster of Excellence, EXC 2193). We would like to thank Dr. Harald Scherer and Fadime Bitgül for the measurement of the NMR spectra, Dr. Thilo Ludwig and Dr. Michael Daub (livMatS) for the measurement and the help with the p-XRD spectra, Daniela Mössner for the measurement of the XPS-spectra and M. Sc. Jan Büttner (livMatS) for the introduction into XPS-spectroscopy. Open Access funding enabled and organized by Projekt DEAL.

## Conflict of Interest

The authors declare no conflict of interest.

## Data Availability Statement

The data that support the findings of this study are available in the supplementary material of this article.

**Keywords:** electrochemistry • electrolyte • magnesium batteries • perfluorinated alkoxy aluminates • weakly coordinating anions

- [1] W. M. Haynes (Ed.) *CRC handbook of chemistry and physics. A ready-reference book of chemical and physical data*, CRC Press, Boca Raton, London, New York, 2017.
- [2] a) J. Muldoon, C. B. Bucur, A. G. Oliver, T. Sugimoto, M. Matsui, H. S. Kim, G. D. Allred, J. Zajicek, Y. Kotani, *Energy Environ. Sci.* **2012**, *5*, 5941; b) J. Song, E. Sahadeo, M. Noked, S. B. Lee, *J. Phys. Chem. Lett.* **2016**, *7*, 1736.
- [3] T. J. Carter, R. Mohtadi, T. S. Arthur, F. Mizuno, R. Zhang, S. Shirai, J. W. Kampf, *Angew. Chem.* **2014**, *126*, 3237.
- [4] Z. Zhao-Karger, M. E. Gil Bardaji, O. Fuhr, M. Fichtner, *J. Mater. Chem. A* **2017**, *5*, 10815.
- [5] C. B. Bucur, T. Gregory, A. G. Oliver, J. Muldoon, *J. Phys. Chem. Lett.* **2015**, *6*, 3578.
- [6] L. W. Gaddum, H. E. French, *J. Am. Chem. Soc.* **1927**, *49*, 1295.
- [7] T. D. Gregory, R. J. Hoffman, R. C. Winterton, *J. Electrochem. Soc.* **1990**, *137*, 775.
- [8] a) D. Aurbach, Z. Lu, A. Schechter, Y. Gofer, H. Gizbar, R. Turgeman, Y. Cohen, M. Moshkovich, E. Levi, *Nature* **2000**, *407*, 724; b) H. Gizbar, Y. Vestfrid, O. Chusid, Y. Gofer, H. E. Gottlieb, V. Marks, D. Aurbach, *Organometallics* **2004**, *23*, 3826; c) D. Aurbach, H. Gizbar, A. Schechter, O. Chusid, H. E. Gottlieb, Y. Gofer, I. Goldberg, *J. Electrochem. Soc.* **2002**, *149*, A115-A121.
- [9] P. Saha, P. H. Jampani, M. K. Datta, C. U. Okoli, A. Manivannan, P. N. Kumta, *J. Electrochem. Soc.* **2014**, *161*, A593-A598.
- [10] a) O. Mizrahi, N. Amir, E. Pollak, O. Chusid, V. Marks, H. Gottlieb, L. Larush, E. Zinigrad, D. Aurbach, *J. Electrochem. Soc.* **2008**, *155*, A103-A109; b) D. Aurbach, G. S. Suresh, E. Levi, A. Mitelman, O. Mizrahi, O. Chusid, M. Brunelli, *Adv. Mater.* **2007**, *19*, 4260.
- [11] a) C. Liebenow, Z. Yang, P. Lobitz, *Electrochem. Commun.* **2000**, *2*, 641; b) H. S. Kim, T. S. Arthur, G. D. Allred, J. Zajicek, J. G. Newman, A. E. Rodnyansky, A. G. Oliver, W. C. Boggess, J. Muldoon, *Nat. Commun.* **2011**, *2*, 427.
- [12] I. Krossing, *Chemistry* **2001**, *7*, 490.
- [13] M. Rohde, P. Eiden, V. Leppert, M. Schmidt, A. Garsuch, G. Semrau, I. Krossing, *ChemPhysChem* **2015**, *16*, 666.
- [14] a) S. Bulut, P. Klose, I. Krossing, *Dalton Trans.* **2011**, *40*, 8114; b) I. M. Riddlestone, A. Kraft, J. Schaefer, I. Krossing, *Angew. Chem. Int. Ed.* **2018**, *57*, 13982; c) H. Böhrer, N. Trapp, D. Himmel, M. Schleip, I. Krossing, *Dalton Trans.* **2015**, *44*, 7489.
- [15] A. B. A. Rupp, I. Krossing, *Acc. Chem. Res.* **2015**, *48*, 2537.
- [16] I. Krossing in *Comprehensive inorganic chemistry II. From elements to applications* (Ed.: J. Reedijk), Elsevier, Amsterdam, 2013, pp. 681–705.
- [17] R. Mohtadi, M. Matsui, T. S. Arthur, S.-J. Hwang, *Angew. Chem. Int. Ed.* **2012**, *51*, 9780.
- [18] O. Tutusaus, R. Mohtadi, T. S. Arthur, F. Mizuno, E. G. Nelson, Y. V. Sevryugina, *Angew. Chem. Int. Ed.* **2015**, *54*, 7900.
- [19] a) S. P. Fisher, A. W. Tomich, S. O. Lovera, J. F. Kleinsasser, J. Guo, M. J. Asay, H. M. Nelson, V. Lavallo, *Chem. Rev.* **2019**, *119*, 8262; b) R. Jay, A. W. Tomich, J. Zhang, Y. Zhao, A. de Gorostiza, V. Lavallo, J. Guo, *ACS Appl. Mater. Interfaces* **2019**, *11*, 11414; c) S. G. McArthur, R. Jay, L. Geng, J. Guo, V. Lavallo, *Chem. Commun.* **2017**, *53*, 4453.
- [20] Z. Zhao-Karger, R. Liu, W. Dai, Z. Li, T. Diemant, B. P. Vinayan, C. Bonatto Minella, X. Yu, A. Manthiram, R. J. Behm et al., *ACS Energy Lett.* **2018**, *3*, 2005.
- [21] J. T. Herb, C. A. Nist-Lund, C. B. Arnold, *ACS Energy Lett.* **2016**, *1*, 1227.
- [22] T. Pavčnik, M. Ložinšek, K. Pirnat, A. Vizintin, T. Mandai, D. Aurbach, R. Dominko, J. Bitenc, *ACS Appl. Mater. Interfaces* **2022**, *14*, 26766-26774.
- [23] a) T. Mandai, Y. Youn, Y. Tateyama, *Mater. Adv.* **2021**, *2*, 6283; b) W. Ren, Di Wu, Y. NuLi, D. Zhang, Y. Yang, Y. Wang, J. Wang, *ACS Energy Lett.* **2021**, *6*, 3212; c) K. Tang, A. Du, X. Du, S. Dong, C. Lu, Z. Cui, L. Li, G. Ding, F. Chen, X. Zhou et al., *Small* **2020**, *16*, e2005424.
- [24] P. Jankowski, Z. Li, Z. Zhao-Karger, T. Diemant, M. Fichtner, T. Vegge, J. M. G. Lastra, *Energy Storage Mater.* **2022**, *45*, 1133.
- [25] a) T. J. Barbarich, S. T. Handy, S. M. Miller, O. P. Anderson, P. A. Grieco, S. H. Strauss, *Organometallics* **1996**, *15*, 3776; b) T. J. Barbarich, S. M. Miller, O. P. Anderson, S. H. Strauss, *J. Mol. Catal. A* **1998**, *128*, 289; c) S. M. Ivanova, B. G. Nolan, Y. Kobayashi, S. M. Miller, O. P. Anderson, S. H. Strauss, *Chemistry* **2001**, *7*, 503.
- [26] a) I. Krossing, H. Brands, R. Feuerhake, S. Koenig, *J. Fluorine Chem.* **2001**, *112*, 83; b) S. Bulut, P. Klose, M.-M. Huang, H. Weingärtner, P. J. Dyson, G. Laurenczy, C. Friedrich, J. Menz, K. Kümmeler, I. Krossing, *Chemistry* **2010**, *16*, 13139.
- [27] I. Raabe, K. Wagner, K. Guttsche, M. Wang, M. Grätzel, G. Santiso-Quiñones, I. Krossing, *Chemistry* **2009**, *15*, 1966.
- [28] T. A. Engesser, M. R. Lichtenhaler, M. Schleip, I. Krossing, *Chem. Soc. Rev.* **2016**, *45*, 789.
- [29] a) A. Shyamsunder, W. Beichel, P. Klose, Q. Pang, H. Scherer, A. Hoffmann, G. K. Murphy, I. Krossing, L. F. Nazar, *Angew. Chem. Int. Ed.* **2017**, *56*, 6192; b) B. G. Nolan, S. H. Strauss, *J. Electrochem. Soc.* **2003**, *150*, A1726-A1734; c) H. Tokuda, M. Watanabe, *Electrochim. Acta* **2003**, *48*, 2085.
- [30] S. Tsujioka, B. G. Nolan, H. Takase, B. P. Fauber, S. H. Strauss, *J. Electrochem. Soc.* **2004**, *151*, A1418-A1423.
- [31] M. P. Stewart, L. M. Paradee, I. Raabe, N. Trapp, J. S. Slattery, I. Krossing, W. E. Geiger, *J. Fluorine Chem.* **2010**, *131*, 1091.
- [32] K.-C. Lau, T. J. Seguin, E. V. Carino, N. T. Hahn, J. G. Connell, B. J. Ingram, K. A. Persson, K. R. Zavadil, C. Liao, *J. Electrochem. Soc.* **2019**, *166*, A1510-A1519.
- [33] E. N. Keyzer, J. Lee, Z. Liu, A. D. Bond, D. S. Wright, C. P. Grey, *J. Mater. Chem. A* **2019**, *7*, 2677.
- [34] T. A. Engesser, C. Friedmann, A. Martens, D. Kratzert, P. J. Malinowski, I. Krossing, *Chemistry* **2016**, *22*, 15085.
- [35] M. Schorpp, I. Krossing, *Chem. Sci.* **2020**, *11*, 2068.
- [36] E. N. Keyzer, H. F. J. Glass, Z. Liu, P. M. Bayley, S. E. Dutton, C. P. Grey, D. S. Wright, *J. Am. Chem. Soc.* **2016**, *138*, 8682.
- [37] I. Krossing, I. Raabe, *Angew. Chem. Int. Ed.* **2004**, *43*, 2066.
- [38] B. Pan, J. Huang, Z. Feng, L. Zeng, M. He, L. Zhang, J. T. Vaughney, M. J. Bedzyk, P. Fenter, Z. Zhang et al., *Adv. Energy Mater.* **2016**, *6*, 1600140.
- [39] a) J. P. H. Li, X. Zhou, Y. Pang, L. Zhu, E. I. Vovk, L. Cong, A. P. van Bavel, S. Li, Y. Yang, *Phys. Chem. Chem. Phys.* **2019**, *21*, 22351; b) S. Oswald, F. Thoss, M. Zier, M. Hoffmann, T. Jaumann, M. Herklotz, K. Nikolowski, F. Scheiba, M. Kohl, L. Giebel, D. Mikhailova, H. Ehrenberg, *Batteries* **2018**, *4*, 36; c) M. Z. Atashbar, H. T. Sun, B. Gong, W. Włodarski, R. Lamb, *Thin Solid Films* **1998**, *326*, 238.
- [40] See for example: a) R. Mohtadi, O. Tutusaus, T. S. Arthur, Z. Zhao-Karger, M. Fichtner, *Joule* **2021**, *5*, 581; b) J. Popovic, *Nat. Commun.* **2021**, *12*, 6240; c) S.-B. Son, T. Gao, S. P. Harvey, K. X. Steirer, A. Stokes, A. Norman, C. Wang, A. Cresce, K. Xu, C. Ban, *Nat. Chem.* **2018**, *10*, 532; d) H. Dou, X. Zhao, Y. Zhang, W. Zhao, Y. Yan, Z.-F. Ma, X. Wang, X. Yang, *Nano Energy* **2021**, *86*, 106087; e) J. Z. Hu, N. R. Jaegers, Y. Chen, K. S. Han, H. Wang, V. Murugesan, K. T. Mueller, *ACS Appl. Mater. Interfaces* **2019**, *11*, 38689; f) R. Mohtadi, *Molecules* **2020**, *25*; g) T. J. Seguin, N. T. Hahn, K. R. Zavadil, K. A. Persson, *Front. Chem.* **2019**, *7*, 175; h) Y. Yu, A. Baskin, C. Valero-Vidal, N. T. Hahn, Q. Liu, K. R. Zavadil, B. W. Eichhorn, D. Prendergast, E. J. Crumlin, *Chem. Mater.* **2017**, *29*, 8504.

Manuscript received: August 1, 2022

Revised manuscript received: September 7, 2022

Accepted manuscript online: September 12, 2022

Version of record online: October 17, 2022